Microscopic mobilities and cooling dynamics of photoexcited carriers in polycrystalline $CuInSe_2$

C. Strothkämper,* A. Bartelt, R. Eichberger, C. Kaufmann, and T. Unold†
Helmholtz-Center Berlin for Materials and Energy, Hahn-Meitner-Platz 1, D-14109 Berlin, Germany
(Received 16 October 2013; revised manuscript received 3 March 2014; published 24 March 2014)

The relaxation and transport dynamics of photoexcited carriers in *p*-type stoichiometric polycrystalline $CuInSe_2$ is investigated by optical-pump terahertz-probe spectroscopy. For all time delays and temperatures studied, the optically measured photoconductivity exhibits a characteristic free carrier Drude response, which allows analyzing the carrier scattering and relaxation phenomena in detail. The hot carrier distribution initially present after photoexcitation is found to relax within the first 200 ps by electron-phonon interaction with polar longitudinal optical (LO) phonons. The relaxed carrier distribution found after 200 ps indicates room temperature minority carrier mobilities close to 1000 cm^2/Vs, in excellent agreement with Hall effect carrier mobilities previously determined for *n*-type single crystals. Analysis of the temperature dependence shows that the mobility at low temperatures is limited by ionized impurity scattering, while at room temperature the scattering of electrons with polar LO phonons dominates.

DOI: 10.1103/PhysRevB.89.115204 PACS number(s): 78.47.db, 72.20.−i, 71.38.−k

I. INTRODUCTION

A fundamental understanding of the carrier dynamics in photoexcited semiconductor materials is of importance for many device applications such as light-emitting diodes, lasers, photodetectors, and solar cells. Compound semiconductors such as $Cu(In,Ga)Se_2$ have become important absorber materials for thin film solar cells, particularly due to the direct optical band gap, with photoconversion efficiencies up to 20.3% [1]. Although in these devices the diffusion lengths play a critical role in achieving high conversion efficiencies, the transport properties are poorly understood, in particular because of the polycrystalline nature of many thin film solar cell materials. Macroscopic transport measurements in general are dominated by transport across grain boundaries, which can lead to a severe underestimation of the intragrain transport properties. Intragrain mobilities may, however, play a key role in solar cell materials, as the typical grain sizes are often comparable to the absorber layer thickness. In addition, Hall effect measurements are dominated by the majority carrier properties, whereas minority carriers play the key role in photovoltaic devices. For example $Cu(In,Ga)Se_2$ thin films used in high-efficiency solar cells are *p* type, which means that the diffusion lengths of electrons, and hence the electron mobilities and lifetimes, are the most important material parameters determining the carrier collection. Thus, in order to determine intragrain mobilities by Hall measurements, *n*-type single crystals have to be studied, which may possess significantly different properties than polycrystalline *p*-type materials. A number of studies have reported Hall measurements on single crystal *n*-type and *p*-type $CuInSe_2$ and $CuGaSe_2$, where room temperature electron mobilities up to 1000 cm^2/Vs and hole mobilities between 3 and ∼300 cm^2/Vs have been found [2–9]. On the other hand, electron mobilities derived from electrical measurements on polycrystalline $Cu(In,Ga)Se_2$ thin films range from 0.02 cm^2/Vs to about 20 cm^2/Vs [10–12]. Electrical measurements show a thermally activated mobility [10,11,13] for polycrystalline $CuInSe_2$, which indicates that the transport properties in these materials are indeed dominated by their grain boundary properties.

In the present study, the scattering mechanisms limiting minority carrier transport in stoichiometric polycrystalline $CuInSe_2$ thin films are investigated using optical-pump terahertz-probe (OPTP) spectroscopy, which serves as a microscopic probe for the charge carrier mobilities within the $CuInSe_2$ crystallites. Although high-efficiency chalcopyrite solar cells use $Cu(In,Ga)Se_2$ absorber layers with typical compositions of $Ga/(In + Ga) \approx 0.3$ and $Cu/(In + Ga) \approx 0.85$, that is, they are strongly copper deficient, we investigate stoichiometric $CuInSe_2$ here as a model system that contains much fewer lattice defects and neither exhibits compositional gradients nor shows signatures of potential fluctuations in its optical properties. Although the defects and composition gradients may have a significant effect on the transport properties in such materials yielding high-efficiency solar cells, we believe that an initial study of the much more simple and well-defined stoichiometric ternary system is necessary for laying the foundations for understanding charge transport in the much more complicated Cu-deficient quaternary system. As will be discussed below, we find that the terahertz photoconductivity in stoichiometric $CuInSe_2$ exhibits a Drude response representative of a free charge carrier response, which allows a detailed modeling of the mobility within the crystallites, yielding important insights into the microscopic bulk scattering mechanisms in this material. For this study, we chose not to perform electrical (e.g., Hall) measurements since, as stated above, these measurement are always found to be dominated by transport across grain boundaries, and they only characterize majority carrier transport. In addition, for reliable Hall measurements, Ohmic contacts are required, which are generally not easy to achieve on chalcopyrite thin films and pose a task that was not in the focus of this study.

The paper is organized as follows. In Sec. II, the experimental details of the samples and the optical setup are given. In Sec. III, the experimental results from the OPTP

*Corresponding author: christian.strothkaemper@helmholtz-berlin.de
†Corresponding author: unold@helmholtz-berlin.de

spectroscopy are presented. In Sec. IV, the theoretical details needed to model the data are introduced. In Sec. V, the modeled temperature and time dependencies are discussed, and in Sec. VI, the main findings are summarized.

II. EXPERIMENTAL DETAILS

Polycrystalline $CuInSe_2$ was grown by coevaporation from elemental sources in a high-vacuum system onto *c*-oriented sapphire substrates. Sapphire is transparent to terahertz radiation and offers good thermal conductivity and a similar thermal expansion as $CuInSe_2$ [14,15]. In a first process stage, Se and In were evaporated at a substrate temperature of $T_1 = 330\,^{\circ}\mathrm{C}$ followed by the evaporation of Se and Cu at a substrate temperature of $T_2 = 550\,^{\circ}\mathrm{C}$ until the material became nominally Cu rich. After the cool down, a KCN treatment was applied to the grown film in order to etch copper selenide secondary phases off the surface [16]. The remaining polycrystalline chalcopyrite thin films are approximately 1-μm thick with grain sizes on the order of 500 nm (see also Fig. S1 in the Supplemental Material [17]), showing stoichiometric composition (Cu $\approx 25 \pm 1$ at.%, In $\approx 25 \pm 1$ at.%, and Se $\approx 50 \pm 1$ at.%) as determined from x-ray fluorescence measurements. Degradation effects were minimized by mounting the samples in a continuous flow cryostat (modified Janis ST-100-FTIR) immediately following the KCN treatment and performing all measurements under high vacuum conditions [18,19]. Low temperature photoluminescence measurements showed sharp donor-acceptor and excitonic peaks typically observed for stoichiometric $CuInSe_2$ (see also Fig. S2 in the Supplemental Material [17]). Companion samples were grown on soda lime glass with and without a molybdenum back contact layer and showed a comparable photoluminescence response. Room temperature OPTP measurements were performed on a number of different samples grown under comparable growth conditions and were found to yield a comparable terahertz response, as reported for one sample in detail in this paper (see also Fig. S3 in the Supplemental Material [17]).

The OPTP spectrometer has been described previously [20]. Laser pulses with a center wavelength of 800 nm and a spot size of 3 mm were used to excite the sample with a fluence of 1.4×10^{12} cm^{-2}. The penetration depth of 800 nm light in stoichiometric $CuInSe_2$ is about 130 nm [21] and thus several times smaller than the sample thickness, so that practically all pump light is absorbed. Averaged over the absorption length, the photoexcitation yields an excess electron concentration of 5×10^{16} cm^{-2}. Far infrared pulses with a bandwidth of about 2 THz and a spot size of 1 mm were used for probing the photoexcited sample and yielded the photoconductivity $\Delta\sigma(\omega,\tau)$ as a function of frequency and pump-probe delay [22,23]. Since both electrons and holes contribute to the photoconductivity $\Delta\sigma = e(n_e\mu_e + n_h\mu_h)$, in principle both carrier types contribute in the OPTP measurement. Here, $n_{e,h}$ and $\mu_{e,h}$ denote the excess density and mobility of electrons (e) and holes (h), respectively, while e is the elementary charge. In the following, the results are discussed assuming dominant electron contribution, which we think is justified because studies that report on both, the electron and the hole mobility, observe 1–2 orders of magnitude higher electron mobility [2,4,7,24].

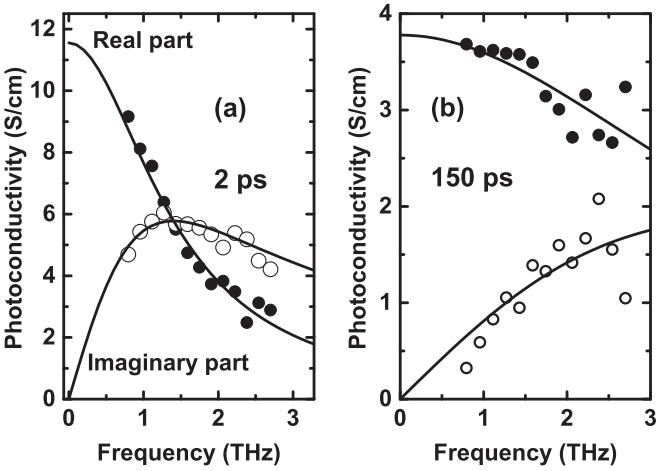

FIG. 1. Terahertz photoconductivity of microcrystalline $CuInSe_2$ at 5 K and two different pump-probe delays of 2 ps (a) and 150 ps (b). The solid lines are a fit with the Drude model, yielding $\tau_D = 113$ fs (a) and $\tau_D = 36$ fs (b).

III. RESULTS

The terahertz spectrum of the photoconductivity $\Delta\sigma$ and hence the mobility $\mu = \Delta\sigma/(n\,e)$ of free charge carriers with density n can be described by the Drude model as [25]

$$\Delta\sigma(\omega) = ne\mu = \frac{ne^2}{m^*}\frac{\tau_D}{1 - i\omega\tau_D}, \tag{1}$$

where m^* denotes the electron effective mass and τ_D is the momentum relaxation time. In Fig. 1, the 5 K photoconductivity spectra recorded at 2 ps and 150 ps after the photoexcitation are shown together with a fit using Eq. (1). It can be seen that for both time delays following photoexcitation of carriers, the terahertz photoconductivity exhibits a frequency dispersion that follows the functional form of the Drude model. In fact, in the present study Drude-like photoconductivities were found from room temperature down to liquid helium temperature and all pump-probe time delays (1.5 ps–1 ns).

This Drude response demonstrates that the majority of electrons remain unbound even at cryogenic temperatures, which is different from the results obtained for other materials such as silicon and ZnO. For these materials OPTP at cryogenic temperatures revealed exciton formation on a 100 ps timescale after the photoexcitation [26,27]. Furthermore, the terahertz photoconductivity is unaffected by grain boundary scattering, as this process would also lead to a distortion of the Drude frequency dispersion [28]. Hence, the observed terahertz photoconductivity is limited by bulk scattering processes and thus allows probing the intragrain transport mechanisms. In the following discussion, we present the mobility as $\mu = e\,\tau_D/m^*$ using the relaxation time τ_D obtained from fits of Eq. (1) to the measured photoconductivity spectra, and the effective electron mass of $m^* = 0.085 m_e$ consistent with literature [29,30].

Figure 2(a) shows the time-resolved relaxation of the mobility following photoexcitation for different temperatures. It can be seen that at a measurement temperature of 5 K, the mobility decays strongly from about 2350 to 800 cm^2/Vs within the first 200 ps. Beyond 200 ps and on the nanosecond timescale, only little changes are observed, indicating that the

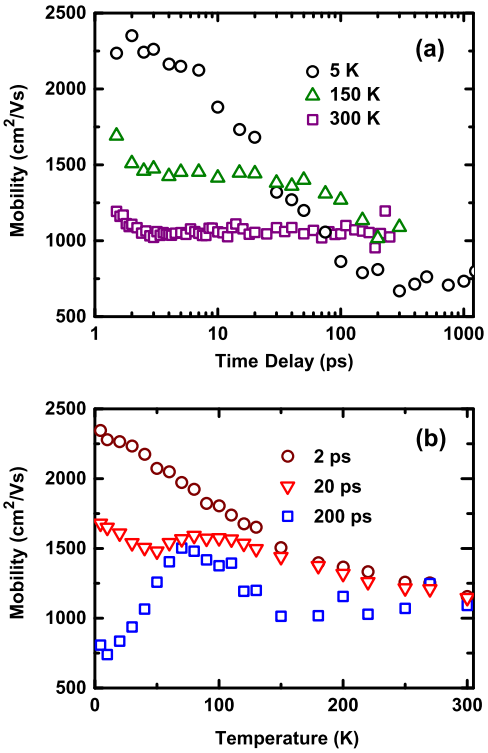

FIG. 2. (Color online) (a) Mobility relaxation curves measured at 5 K, 150 K, and 300 K. (b) Temperature-dependent experimental mobilities at delay times of 2 ps, 20 ps, and 200 ps.

electrons have almost reached equilibrium with the lattice at this pump-probe delay. On the other hand, for measurement temperatures close to room temperature, the mobility exhibits only a small decay over the first 2 ps and then remains constant. Figure 2(b) exhibits the mobility as a function of the sample temperature for pump-probe delays of $\Delta t = 2$ ps, 20 ps, and 200 ps. As expected from Fig. 2(a), the mobilities are essentially independent of the time delay at room temperature and amount to 1100 cm^2/Vs, which is comparable to the highest values measured on n-type single crystalline samples [2–6] (see also Fig. S4 in the Supplemental Material [17]).

With decreasing temperature, the mobilities at short and long time delays show a fundamentally different behavior. At a short time delay of 2 ps, the mobility increases almost linearly with decreasing temperature to a maximum value of 2350 cm^2/Vs at 5 K. In contrast, 200 ps after the excitation pulse, the mobility exhibits a maximum at ∼80 K and decreases for lower temperatures toward ∼750 cm^2/Vs at 5 K. For an intermediate time delay of 20 ps, the mobility values are in between those of the 2 ps and 200 ps mobilities for all temperatures. The qualitative trend of the mobility at 200 ps time delay has been observed in transport measurements of various semiconductors and has been generally explained by phonon scattering at high temperatures and ionized impurity scattering at low temperatures. A similar behavior was observed in several studies of the Hall mobility in $CuInSe_2$ single crystals and thin films [2,4,5,13,24]. Together with the mobility relaxation transients shown in Fig. 2, these results indicate that the terahertz mobilities measured at 200 ps time delay correspond to a steady-state situation similar to dc transport measurements. In contrast, the behavior immediately following photoexcitation (2 ps time delay) is strongly influenced by the excess energy gained from the excitation, i.e., an electron temperature T_e, which is higher than the sample temperature T_l. At low sample temperatures when phonons are frozen, the higher T_e reduces ionized impurity scattering and thus increases the mobility. A rough estimate of the hot electron temperature at low sample temperature can be made by comparing the difference of the hot electron mobility (2 ps) and the relaxed mobility (200 ps) with the temperature-dependent variation of the relaxed mobility. Using this approximation, it can be estimated that the electron temperature T_e at 2 ps and 5 K is more than 100 K higher than the lattice temperature.

In the following, we first discuss the mobility of relaxed electrons (long time delays) and then continue with the cooling dynamics and the hot electron mobility.

IV. MODELING AND DISCUSSION

The mechanisms that have to be taken into account to model the mobility are ionized impurity and electron-phonon scattering. The latter process includes acoustic deformation potential scattering with longitudinal acoustic (LA) phonons and the polar interaction with longitudinal optical (LO) phonons. Deformation potential scattering with optical phonons does not have to be taken into account here because it does not occur for the s-type conduction band wavefunctions in $CuInSe_2$ [6]. The mobility due to ionized impurity and acoustic deformation potential scattering may be calculated from the relaxation time approximation of the Boltzmann equation as [31]

$$\mu = \frac{2\sqrt{2m^*}e}{3\pi^2\hbar^3 n} \cdot \int E^{3/2}\tau_D \cdot \frac{\partial f}{\partial E} dE, \tag{2}$$

where f is the Fermi-Dirac occupation probability, E is the energy of photoexcited electrons with density n and effective mass m^*, and $\tau_D = \tau_D(E(\mathbf{k}))$ is the energy-dependent momentum relaxation time. The latter is given as [31]

$$\frac{1}{\tau_D(k)} = \frac{1}{4\pi^2\hbar} \int |M_q|^2(1-\cos(\theta))\,\delta(E_{\mathbf{k}'} - E_{\mathbf{k}})d\mathbf{k}'. \tag{3}$$

In Eq. (3), θ is the angle between $\mathbf{k}$ and $\mathbf{k}'$, the electron wavevector before and after a scattering event. For scattering with acoustic phonons, the matrix elements $|M_q|^2$ are

$$|M_q|^2 = \begin{pmatrix} N_q \\ N_q + 1 \end{pmatrix} \frac{\hbar q}{2\rho v_l} E_{ac}^2, \tag{4}$$

where ρ (=5.77 g/cm^3), v_l, and E_{ac} denote the mass density, velocity of sound of the LA phonons, and the deformation potential, respectively. For the LA phonon group velocity, a value of 3770 m/s was used [32]. In Eq. (4) and in the following, upper and lower symbols denote absorption and emission of a phonon with occupation number N_q and wavevector $\mathbf{q} = \pm(\mathbf{k} - \mathbf{k}')$.

For scattering with ionized impurities, we use the Brooks-Herring approximation [31]

$$|M_q|^2 = \frac{n_I e^4}{\varepsilon(0)^2} \frac{1}{\left(q_0^2 + q^2\right)^2}, \tag{5}$$

where n_I, $\varepsilon(0)$, $q_0 = (4\pi^2/\varepsilon(0) \cdot \partial n/\partial E_F)^{1/2}$, and E_F denote the density of ionized impurities, the permittivity, the inverse

screening length, and the Fermi level, respectively. The mobility limited by the polar interaction with LO phonons is approximated following Conwell [33] by averaging the momentum change in the direction of an applied field E_0

$$\frac{dp(k)}{dt} = \frac{1}{4\pi^2\hbar}\int \frac{\mathbf{E}_0(\pm\hbar\mathbf{q})}{E_0}|M_q|^2\,\delta(E_{\mathbf{k}\pm\mathbf{q}} - E_{\mathbf{k}} \mp \hbar\omega)d\mathbf{q} \tag{6}$$

over a drifted Maxwell-Boltzmann distribution. As a result, the average momentum loss rate can be related to the drift velocity $\langle dp/dt\rangle \propto v_d$. The mobility then follows from $\langle dp/dt\rangle = -eE_0$ and the relation $\mu = v_D/E_0$. The matrix elements for the polar interaction in Eq. (6) are given by [31]

$$|M_q|^2 = \frac{e^2\hbar\omega}{2}\left(\frac{1}{\varepsilon(\infty)} - \frac{1}{\varepsilon(0)}\right)\binom{N_q}{N_q+1}\frac{q^2}{\left(q_0^2+q^2\right)^2}. \tag{7}$$

The mobilities from the different scattering mechanisms are combined by Matthiessen's rule

$$\frac{1}{\mu} = \frac{1}{\mu_{\text{ion}}} + \frac{1}{\mu_{\text{opt}}} + \frac{1}{\mu_{\text{ac}}}, \tag{8}$$

yielding the result $\mu = \mu(T_e, T_l)$, which is a function of the lattice and electron temperature through the dependence of the electron scattering rates on the phonon occupation numbers $N_q(T_l)$ and the electron energy $\varepsilon(\mathbf{k})$.

The electron-polar LO phonon (Fröhlich) interaction described in Eq. (7) directly depends on the static and high-frequency permittivities $\varepsilon(0)$ and $\varepsilon(\infty)$, characterizing the effective ionic charge [34–37] and determining the polarization field created by the LO phonons. The static and high frequency dielectric constants in $CuInSe_2$ are not exactly known. In the following, values of $\varepsilon(0) = 12$ and $\varepsilon(\infty) = 8$ will be used, which is consistent with recent data from capacitance and ellipsometry measurements [38,39]. We also note that Eq. (7) originally was derived for the specific case of one single LO phonon branch. In $CuInSe_2$, however, nine polar LO phonon branches [40] exist due to its specific crystal symmetry [41]. Although in principle electron-phonon scattering involving all nine LO phonon branches is conceivable, it is not expected that all nine phonon branches equally couple to electrons. An indication for this can be found in typical low temperature photoluminescence spectra where donor-acceptor pair transitions only exhibit 28 meV phonon replica, corresponding to the two almost degenerate highest energy LO phonon branches in $CuInSe_2$ (Ref. [42]). From this we deduce that the electron-phonon interaction with the lower energy LO phonons is comparably weak, and we will only include the two highest energy LO phonon branches in the calculation of the Fröhlich interaction.

For the acoustic deformation potential, a wide range of values (7–55 eV) has been used to fit $CuInSe_2$ transport data in the literature [2,6,13,24]. However, a value for the conduction band deformation potential $E_{ac} = 10$ eV has been independently inferred from the band gap temperature dependence in $CuInSe_2$ [43–45], which is in good agreement with the deformation potentials deduced for a large number of compound semiconductors [46]. The ionized impurity density in the electron-ionized impurity scattering probability is *a priori* unknown for our films and is thus a free fit parameter.

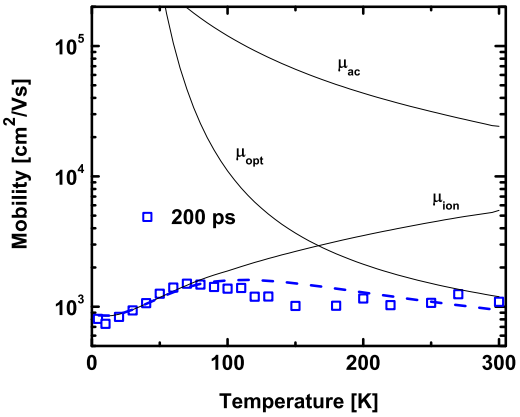

FIG. 3. (Color online) Experimental terahertz mobility at 200 ps and calculated mobility (dashed line) with the different contributions (thin solid lines).

As shown in Fig. 3, the characteristic dependence of the thermalized electron mobility (time delay of $\Delta t = 200$ ps) on temperature can be reasonably well reproduced assuming an ionized impurity density $n_I = 3\times10^{17}$ cm^{-3} and the material parameters detailed above. It can be seen that at low temperatures impurity scattering excellently describes the temperature dependence of the relaxed terahertz mobility. At high temperatures around room temperature, electron-phonon scattering by polar LO phonons clearly limits the mobility, as is generally expected for polar semiconductors. It can also be seen that acoustic deformation potential scattering does not play any significant role in limiting the free carrier mobility in these polycrystalline $CuInSe_2$ thin films, in contrast to previous conclusions in the literature [4,13,24]. In a number of these previous findings, unrealistically large acoustic deformation potential values were assumed (up to 55 eV in Ref. [2]), or optical deformation potential scattering was assumed [2,4,13,24]. Also, only one polar LO-phonon branch was considered, which overestimates the mobility due to electron-LO phonon scattering.

If the carrier scattering processes considered above correctly describe the electron mobility in $CuInSe_2$, they should also allow a description of the time dependence of the mobility observed in Fig. 2(a). Photoexcitation of electron-hole pairs at energies in excess of the band gap energy leads to the generation of hot electrons and holes, which subsequently cool by the emission of phonons until they are equilibrated with the lattice. In particular, at low temperatures the mobility is strongly enhanced at short time delays after the pump pulse because impurity scattering is reduced for the hot electrons, and at the same time phonon scattering is weak because the phonons are frozen in. With the cooling of the hot electrons, the mobility decreases due to increased scattering with ionized impurities and phonons generated by the cooling processes.

The electron cooling dynamics depends on the net rate of phonon emission. At long time delays, when electrons and phonons are thermalized, phonon absorption and emission balance each other. However, in the case of hot carriers, phonon emission dominates, and there is a net energy transfer to the

lattice. Phonon emission and absorption change the phonon occupancy for a given mode according to [47]

$$\frac{dN_q}{dt} = \pm\frac{1}{2\pi^2\hbar}\int |M_q|^2 f_{\mathbf{k}}\,(f_{\mathbf{k}\pm\mathbf{q}})\delta(E_{\mathbf{k}\pm\mathbf{q}} - E_{\mathbf{k}} \mp \hbar\omega)d\mathbf{k} - \frac{N_q - N_q(T_l)}{\tau_l}, \tag{9}$$

where the last term in Eq. (9) describes the relaxation of the nonequilibrium population N_q to the equilibrium value $N_q(T_l)$, with a decay time of τ_l due to the decay of optical phonons into acoustic phonons [48]. Considering energy conservation, the electron energy loss is obtained from the energy gain by the phonons

$$\frac{dE}{dt} = -\sum_{q,s}\hbar\omega_q\frac{dN_q}{dt}, \tag{10}$$

where s runs over the considered optical and acoustic branches. The change of the electron temperature then follows from

$$\frac{dT_e}{dt} = \frac{dE(T_e(t))}{dt}\Big/\frac{dE(T_e)}{dT_e}. \tag{11}$$

Here, the temperature dependence of the total energy of the electron ensemble can be explicitly stated as

$$\frac{dE(T_e)}{dT_e} = \int E\cdot D(E)\frac{df(E;E_F,T_e)}{dT_e}dE \tag{12}$$

with the density of states $D(E)$ and (quasi-) Fermi level E_F. The Fermi level itself is temperature dependent, and this dependence must be known to calculate df/dT_e in Eq. (12). It is obtained from numerically solving

$$\int D(E)f(E;E_F(T_e),T_e)dE = n, \tag{13}$$

where $n \approx 5\times10^{16}\mathrm{cm}^{-3}$ is the photoexcitation density averaged over the absorption length. Estimating the initial electron temperature $T_e \approx 2000$ K from the equipartition relation and the assumption that the excess energy is split evenly between electrons and holes, $3/2\,k_B T_e = (\hbar\omega_{\mathrm{pump}} - E_{\mathrm{gap}})/2$, we can obtain $T_e(t)$ from integrating Eq. (11). This methodology approximates the true cooling curve because it neglects the phonon-hole and electron-hole interactions, which are difficult to handle due to the strong anisotropy and nonparabolicity of the valence bands [49].

As can be seen in Fig. 4(a), the calculated electron temperature initially decays rapidly by emission of LO phonons resulting from the Fröhlich interaction and strongly decelerates after about one picosecond due to reabsorption of hot phonons [47,51]. The calculated hot LO phonon occupation, as obtained from Eq. (9), is depicted in the inset in Fig. 4(a) for different time delays. For q values where scattering with electrons occurs most frequently, a plateau evolves over time, indicating that these phonons are in equilibrium with the electrons [47]. The cooling dynamics following the first few picoseconds is mainly limited by the decay rate of hot optical phonons into acoustic phonons. If the increase in the nonequilibrium phonon population is disregarded in the calculation of the cooling curve, which formally corresponds to $\tau_l \to 0$ in Eq. (9), no deceleration of the cooling due to phonon reabsorption occurs,

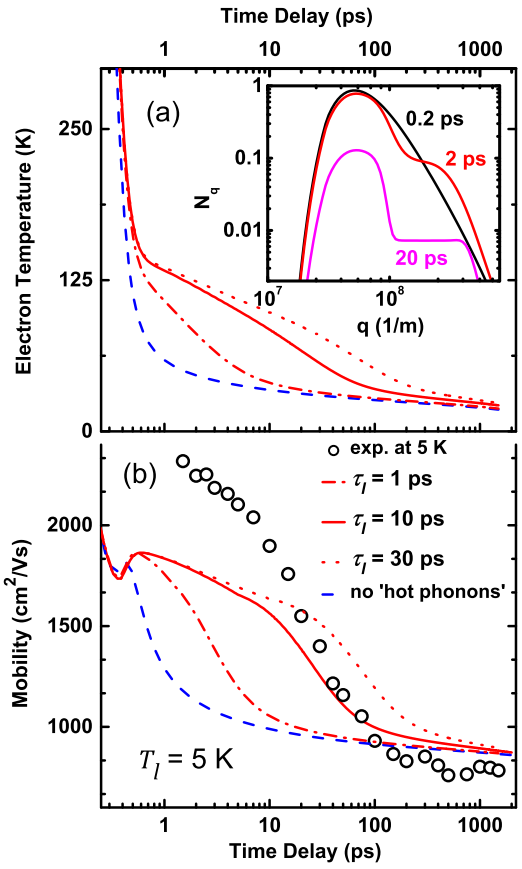

FIG. 4. (Color online) (a) Calculated cooling curves at 5 K for an initial electron temperature of 2000 K at 0 ps and different optical phonon lifetimes. The curve calculated without hot phonons represents the limiting case of an infinitely fast relaxation of the excess optical phonon population, i.e., $\tau_l \to 0$ in Eq. (9). The inset exemplifies the time dependence of the phonon population according to Eq. (9) for an optical phonon decay time of $\tau_l = 10$ ps. (b) Time dependence of the mobility in $CuInSe_2$ at a sample temperature of 5 K and calculated hot electron mobility curves. The mobility spectra cannot be measured for time delays shorter than ~1.5 ps because of frequency artifacts that arise when the conductivity changes rapidly with time (Ref. [50]).

and the cooling proceeds significantly faster, as shown by the dashed line in Fig. 4(a).

Using the calculated electron cooling curve and $N_q(t)$, the time-dependent hot electron mobility $\mu(t) = \mu(T_e(t), N_q(t))$ can be obtained using the formalism described by Eqs. (2)–(8). Consistent with the previously described calculations of the relaxed mobilities ($\Delta t = 200$ ps), we assume for the Fröhlich interaction a predominant coupling to the two highest energy LO phonon modes with $\hbar\omega = 28$ meV. The time-dependent mobilities, which correspond to the cooling curves in Fig. 4(a), are shown in Fig. 4(b). Aside from the inclusion of a nonequilibrium hot phonon population $N_q(t)$, the same carrier scattering parameters as used for the description of the (relaxed) mobility temperature dependence were employed. It can be seen that the relaxation of the hot electron mobility can be qualitatively modeled if the hot phonon distribution is taken into account with a phonon lifetime on the order of 10 ps, which is consistent with low

temperature Raman linewidths found for various adamantine semiconductors [52,53]. In contrast, the agreement is very poor if the phonon lifetime is significantly different from 10 ps or if the nonequilibrium phonon distribution is neglected.

In all cases, the mobility is slightly underestimated for time delays smaller than 20 ps. This cannot be simply due to an overestimation of the electron energy loss at short time delays; thus, an underestimation of the electron temperature because with higher electron temperatures phonon emission becomes so effective that the mobility declines again. On the other hand, it is questionable if during the initial cooling process a thermal equilibrium distribution defining an electron temperature can be assumed. In this case, the evolution of the phonon occupation during this time period is incorrectly described by the formalism outlined above, which can easily lead to deviations in the electron-phonon scattering contribution to the time-dependent mobility. Further experimental and theoretical work is needed to elucidate the exact nature of the carrier-carrier and carrier-phonon interactions on these very short time scales.

V. CONCLUSIONS

Using OPTP, we determined the microscopic mobilities within stoichiometric $CuInSe_2$ grains of polycrystalline $CuInSe_2$ thin films. The terahertz mobility exhibits a Drude behavior, indicating free-electron response. Mobilities between 800 and 2350 cm^2/Vs are found, which are almost equivalent to macroscopically determined mobilities in single-crystalline $CuInSe_2$, indicating that the intragrain transport is only determined by bulk scattering mechanisms reminiscent of single crystals. As contributions from grain boundaries can be neglected, it follows that while grain boundaries may pose a limit to long range transport, the transport inside these individual grains of stoichiometric polycrystalline $CuInSe_2$ is about as efficient as in single crystals. We find that, except for ionized impurity scattering at low temperatures, the mobility is limited by polar optical phonon scattering, and that acoustic deformation potential scattering does not play a significant role. Our results also suggest that the polar interaction of electrons with the optical phonons is dominated by the coupling to the two highest energy (28 meV) LO phonon modes. Although high-efficiency chalcopyrite solar cells use Cu-deficient $Cu(In,Ga)Se_2$ thin films, which may exhibit different material properties than stoichiometric $CuInSe_2$ thin films, these findings are important also for solar cells in that they further the understanding of the fundamental scattering mechanisms and give an upper estimate of electron mobilities achievable in this polycrystalline material system.

[1] P. Jackson, D. Hariskos, E. Lotter, S. Paetel, R. Wuerz, R. Menner, W. Wischmann, and M. Powalla, Prog. Photovoltaics **19**, 894 (2011).

[2] S. M. Wasim, Solar Cells **16**, 289 (1986).

[3] H. Neumann and R. D. Tomlinson, Solar Cells **28**, 301 (1990).

[4] P. Gorley, V. Khomyak, Y. Vorobiev, J. Gonzalez-Hernandez, P. Horley, and O. Galochkina, Solar Energy **82**, 100 (2008).

[5] L. Essaleh, S. M. Wasim, and J. Galibert, J. Appl. Phys. **90**, 3993 (2001).

[6] S. M. Wasim and A. Noguera, Phys. Status Solidi A **82**, 553 (1984).

[7] H. Takenoshita and T. Nakau, Jpn. J. Appl. Phys. **20**, 1333 (1981).

[8] D. J. Schroeder, J. L. Hernandez, G. D. Berry, and A. A. Rockett, J. Appl. Phys. **83**, 1519 (1998).

[9] S. Siebentritt, Thin Solid Films **480**, 312 (2005).

[10] S. M. F. Hasan, M. A. Subhan, and K. M. Mannan, Opt. Mater. **14**, 329 (2000).

[11] Y. Tang, R. Braunstein, and B. von Roedern, Appl. Phys. Lett. **63**, 2393 (1993).

[12] S. A. Dinca, E. A. Schiff, W. N. Shafarman, B. Egaas, R. Noufi, and D. L. Young, Appl. Phys. Lett. **100**, 103901 (2012).

[13] I. Sanyal, K. K. Chattopadhyay, S. Chaudhuri, and A. K. Pal, J. Appl. Phys. **70**, 841 (1991).

[14] A. N. Amatuni and E. B. Shevchenko, Meas. Tech.-USSR **9**, 1256 (1966).

[15] P. Kistaiah, Y. C. Venudhar, K. S. Murthy, L. Iyengar, and K. V. K. Rao, J. Phys. D Appl. Phys. **14**, 1311 (1981).

[16] R. Klenk, R. Menner, D. Cahen, and H. W. Schock, IEEE Phot. Spec. Conf. **1**, 481 (1990).

[17] See Supplemental Material at http://link.aps.org/supplemental/10.1103/PhysRevB.89.115204 for a micrograph, photoluminescence data, OPTP data of additional samples, and a comparison with Hall mobilities from literature.

[18] W. Metzger, I. Repins, M. Romero, P. Dippo, M. Contreras, R. Noufi, and D. Levi, Thin Solid Films **517**, 2360 (2009).

[19] W. K. Metzger, I. L. Repins, and M. A. Contreras, Appl. Phys. Lett. **93**, 022110 (2008).

[20] C. Strothkämper, K. Schwarzburg, R. Schütz, R. Eichberger, and A. Bartelt, J. Phys. Chem. C **116**, 1165 (2012).

[21] M. I. Alonso, K. Wakita, J. Pascual, M. Garriga, and N. Yamamoto, Phys. Rev. B **63**, 075203 (2001).

[22] H. Němec, F. Kadlec, and P. Kužel, J. Chem. Phys. **117**, 8454 (2002).

[23] P. Kuzel, F. Kadlec, and H. Němec, J. Chem. Phys. **127**, 024506 (2007).

[24] T. Irie, S. Endo, and S. Kimura, Jpn. J. Appl. Phys. **18**, 1303 (1979).

[25] H. Němec, P. Kužel, and V. Sundström, J. Photoch. Photobio. A **215**, 123 (2010).

[26] T. Suzuki and R. Shimano, Phys. Rev. B **83**, 085207 (2011).

[27] E. Hendry, M. Koeberg, and M. Bonn, Phys. Rev. B **76**, 045214 (2007).

[28] H. Němec, P. Kužel, and V. Sundström, Phys. Rev. B **79**, 115309 (2009).

[29] H. Weinert, H. Neumann, H.-J. Höbler, G. Kühn, and N. van Nam, Phys. Status Solidi A **81**, K59 (1977).

[30] E. Arushanov, L. Essaleh, J. Galibert, J. Leotin, M. A. Arsene, J. P. Peyrade, and S. Askenazy, Appl. Phys. Lett. **61**, 958 (1992).

[31] C. Jacoboni, *Theory of Electron Transport in Semiconductors* (Springer, Heidelberg, 2010).

[32] B. Fernández and S. M. Wasim, Phys. Status Solidi A **122**, 235 (1990).

[33] E. M. Conwell, *High Field Transport in Semiconductors* (Academic, New York, 1967).
[34] H. B. Callen, Phys. Rev. **76**, 1394 (1949).
[35] H. Ehrenreich, J. Phys. Chem. Solids **2**, 131 (1957).
[36] H. Fröhlich, Adv. Phys. **3**, 325 (1954).
[37] H. Fröhlich, Proc. R. Soc. Lond. A **160**, 230 (1937).
[38] T. Eisenbarth, T. Unold, R. Caballero, C. A. Kaufmann, and H.-W. Schock, J. Appl. Phys. **107**, 034509 (2010).
[39] P. D. Paulson, R. W. Birkmire, and W. N. Shafarman, J. Appl. Phys. **94**, 879 (2003).
[40] C. Parlak and R. Eryiğit, Phys. Rev. B **66**, 165201 (2002).
[41] H. Neumann, Solar Cells **16**, 399 (1986).
[42] M. Wagner, I. Dirnstorfer, D. Hofmann, M. Lampert, F. Karg, and B. Meyer, Phys. Status Solidi A **167**, 131 (1998).
[43] M. Quintero, C. Rincon, R. Tovar, and J. C. Woolley, J. Phys.: Condens. Mat. **4**, 1281 (1992).
[44] C. Rincon and B. Fernandez, Phys. Status Solidi B-Basic Res. **170**, 531 (1992).
[45] C. Rincon and J. Gonzalez, Phys. Rev. B **40**, 8552 (1989).
[46] M. Cardona and N. E. Christensen, Phys. Rev. B **35**, 6182 (1987).
[47] S. S. Prabhu, A. S. Vengurlekar, S. K. Roy, and J. Shah, Phys. Rev. B **51**, 14233 (1995).
[48] B. K. Ridley, *Quantum Processes in Semiconductors* (Oxford University Press, Oxford, 2000).
[49] C. Persson, Appl. Phys. Lett. **93**, 072106 (2008).
[50] H.-K. Nienhuys and V. Sundström, Phys. Rev. B **71**, 235110 (2005).
[51] J. Shah, *Ultrafast Spectroscopy of Semiconductors and Semiconductor Nanostructures* (Springer, Berlin, 1999).
[52] L. Bergman, D. Alexson, P. L. Murphy, R. J. Nemanich, M. Dutta, M. A. Stroscio, C. Balkas, H. Shin, and R. F. Davis, Phys. Rev. B **59**, 12977 (1999).
[53] J. Menéndez and M. Cardona, Phys. Rev. B **29**, 2051 (1984).